Electronic Supplementary Information

Separating photoanode from recognition event: toward a general strategy for self-powered photoelectrochemical immunoassay with both high sensitivity and anti-interference capability

Gao-Chao Fan,† Linzheng Ma,† Jayachandran Silambarasan, Zimeng Li, and Xiliang Luo*

Key Laboratory of Sensor Analysis of Tumor Marker, Ministry of Education, College of Chemistry and Molecular Engineering, Qingdao University of Science and Technology, Qingdao 266042, P. R. China

*E-mail: xiliangluo@qust.edu.cn

Section 1: Experimental

Materials and Reagents. Titanium foil (99.7% purity, 0.25 mm thick), ethylene glycol (EG), ammonia fluoride (NH_4F), 3,4-ethylenedioxythiophene (EDOT), chitosan powder (from crab cells, 85% deacetylation), and bovine serum albumin (BSA) were all obtained from Sigma-Aldrich (USA). ITO electrodes (type JH52, ITO coating 30 ± 5 nm, sheet resistance ≤ 10 Ω/square) were ordered from Nanjing Zhongjingkeyi Technology Co., Ltd. (China). Urea, acetone, ethanol, and sodium hydroxide (NaOH) were obtained from Aladdin reagent Inc. (Shanghai, China). Graphite powder, sulfuric acid (H_2SO_4), hydrochloric acid (HCl), potassium peroxydisulfate ($K_2S_2O_8$), potassium permanganate ($KMnO_4$), phosphorus pentoxide (P_2O_5), glutaraldyhyde (GLD, 25% aqueous solution) and ascorbic acid (AA) were purchased from Sinopharm Chemical Reagent Co., Ltd. (China). Human interleukin-6 (IL-6, Ag), IL-6 antibody (Ab), human interleukin-8 (IL-8), human IgG (HIgG), carcinoembryonic antigen (CEA), and α-fetoprotein (AFP) were obtained from Shanghai Linc-Bio Science Co. Ltd. (China). All other reagents were of analytical grade and used as received. All aqueous solutions were prepared with deionized water (DI water, 18 MΩ/cm), coming from a Milli-Q water purification system. Phosphate buffer solution (PBS, pH 7.4, 10 mM) was used for the preparation of the antibody and antigen solution, washing buffer solution, and blocking buffer solution which contained 1% (w/v) BSA.

Apparatus. Photoelectrochemical measurements were performed with a homebuilt photoelectrochemical system. A 150 W xenon lamp was utilized as the irradiation source with the light intensity of 500 $mW \cdot cm^{-2}$ estimated by a radiometer (Photoelectric Instrument of Beijing Saifan Co., LTD.). Photocurrent was measured on a CHI 760D electrochemical workstation (Shanghai Chenhua Apparatus Corporation, China). X-ray photoelectron spectroscopy (XPS) was performed using an ESCALAB 250Xi spectrometer (Thermo Fisher Scientific, UK) with a monochromatic Al Kα X-ray source, and all spectra were calibrated by normalizing the C (1s) peak to the standard value of 284.6 eV. Field-emission scanning electron microscopy (FE-SEM) was carried out on a Hitachi S-4800 scanning electron microscope (Hitachi Co., Japan). Electrochemical impedance spectroscopy (EIS) was carried out on an Autolab potentiostat/galvanostat (PGSTAT 30, Eco Chemie B.V., Utrecht, Netherlands) with a three-electrode system in 0.1 M KCl solution containing 5.0 mM $K_3[Fe(CN)_6]/K_4[Fe(CN)_6]$ (1:1) mixture as a redox probe, and recorded in the frequency range of 0.01 Hz-100 kHz with an amplitude of 50 mV.

Preparation of TiO_2-NTAs. The TiO_2 nanotube arrays (TiO_2-NTAs) were prepared by a modified two-step anodization process.[1] Prior to anodization, titanium foils were mechanically polished with abrasive papers and rinsed with DI water, and then ultrasonically cleaned in acetone, ethanol and DI water for 10 min, respectively. The anodization was conducted at room temperature in a conventional two-electrode system with a Ti foil as anode and a Pt wire as cathode. The electrolyte of each anodization process was the same, which was composed of 0.5 wt% NH_4F in EG solution with 2 % (v/v) water. In the first-step anodization, the Ti foil was anodized at 40 V for 20 min, followed by removing the as-grown nanotube layer ultrasonically in DI water. Subsequently, the treated Ti foil was anodized at 30 V for 20 min in the second-step anodization. After the two-step anodization, the obtained TiO_2-NTAs sample was cleaned with DI water and dried with N_2 gas, and then was annealed in air at 450 C for 1 h with a heating rate of 5 ºC/min.

Deposition of g-C_3N_4 on TiO_2-NTAs. Deposition of graphitic carbon nitride (g-C_3N_4) on the TiO_2-NTAs electrode was achieved using a facile solid sublimation and transition (SST) process with urea as precursor.[2] Typically, 2.0 g urea was added in a crucible, and the TiO_2-NTAs electrode was placed above the urea powders. The crucible was covered with an aluminum foil and then heated at 550 °C for 4 h at a ramping rate of 8 °C/min in a muffle furnace. During the SST process, a small amount of g-C_3N_4 polymer was deposited onto the TiO_2-NTAs, whereas the majority of the produced g-C_3N_4 powders remained on the bottom of crucible.

Fabrication of TiO_2-NTAs/g-C_3N_4/PEDOT photoanode. The PEC polymerization of poly(3,4-ethylenedioxythiophene) (PEDOT) layer onto the TiO_2-NTAs/g-C_3N_4 electrode was based on literature method.[3] The reaction was occurred in a three-electrode electrochemical system with a TiO_2-NTAs/g-C_3N_4 electrode as working electrode, a Pt-wire as counter electrode, and a saturated calomel electrode as reference electrode. The TiO_2-NTAs/g-C_3N_4 electrode surface was exposed to both the electrolyte and the irradiation, and the optical path of the irradiation source was kept still in the whole process. The polymerization solution contained 0.1 M $LiClO_4$ and 0.01 M monomer of EDOT in acetonitrile, which was deaerated by pure nitrogen for 30 min prior to polymerization. The potentiodynamic deposition technique was employed at a scan rate of 50 mV/s for 3 cycles. Simultaneously with the start of potentiodynamic polymerization, the working electrode was irradiated.

Electrodeposition of RGO on ITO electrode. The graphene oxide (GO) solution was firstly prepared

based on an improved Hummers's method.[4] The electrodeposition of reduced graphene oxide (RGO) was according to the literature method with some modifications.[5] The base solution was 0.8 mg/mL GO dispersion. The cyclic voltammetric reduction was carried out on a CHI 760D electrochemical workstation (CH Instruments, Shanghai) using a three-electrode: the bare ITO with fixed area of 0.25 cm^2 as the working electrode, Pt wire as the counter electrode, and Ag/AgCl as the reference electrode. The scan range was between −1.3 and 0.6 V at a rate of 0.1 V/s. After 30 cycles of scan, the working electrode was rinsed with DI water.

Fabrication of cathodic sensing electrode. Chitosan (CS) solution was prepared by dissolving CS powder in 1% acetic acid, and then 20 μL of 0.1 wt% CS solution was dropped onto the ITO/RGO electrode and was dried at 50 °C. After being rinsed with 0.1 M NaOH and DI water in order, the electrode was cover with 20 μL of 5% GLD and maintained for 30 min. The excessive or physically adsorbed GLD was removed by rinsing the electrode with DI water. Next, 20 μL of 100 μg/mL IL-6 antibodies (Ab) were introduced onto the electrode and incubating at 4 °C for 12 h. After being rinsed with washing buffer solution (PBS, pH 7.4, 10 mM), the electrode was incubated with 20 μL of BSA blocking buffer solution at 37 °C for 30 min to block nonspecific binding sites. Subsequently, the electrode was rinsed with washing buffer solution thoroughly and then incubated with 20 μL of different concentrations of IL-6 antigens (target Ag) at 37 °C for 1 h. After being rinsed with washing buffer solution, the resulting electrode was finally introduced into photocurrent detection.

Photoelectrochemical measurement. The photoelectrochemical experiment was operated with a conventional two-electrode system: a cathode of modified ITO/RGO electrode with an area of 0.25 cm^2 as working electrode, and a photoanode of TiO_2-NTAs/g-C_3N_4/PEDOT with an area of 0.25 cm^2 as counter electrode. The photocurrent determination was carried out at room temperature in PBS (pH 7.4, 0.1 M) containing 0.1 M ascorbic acid (AA), which acted as sacrificial reagents providing electrons to photoanode. A xenon lamp with a spectral range of 300-2500 nm was utilized as irradiation source, which illuminated only on photoanode, and it was switched on and off every 10 s. The electrochemical technique was time-current test, and the applied voltage was 0.0 V. The modified ITO/RGO cathodic electrode was placed behind and in parallel with the TiO_2-NTAs/g-C_3N_4/PEDOT photoanode. As the photoanode substrate of the titanium foil was nontransparent, the illumination could not shine on the cathodic electrode.

Section 2: XPS of the photoanode

In order to further confirm the states of elements and composition information, XPS of the TiO_2-NTAs/g-C_3N_4/PEDOT photoanode during its modification process was characterized, as presented in Fig. S1. It is observed in Panel A that the TiO_2-NTAs is mainly composed of Ti and O elements, and the XPS peak for C 1s is used as the internal reference to correct the binding energy.[6] After g-C_3N_4 layer deposition, as shown in Panel B, the typical N 1s appear. While PEDOT layer deposition, as shown in Panel C, the typical XPS peaks for S 2s and S 2p arise, and the Cl element is derived from the raw materials of $LiClO_4$ during PEC polymerization. Thus, the XPS characterization further proved the successful fabrication of the TiO_2-NTAs/g-C_3N_4/PEDOT photoanode.

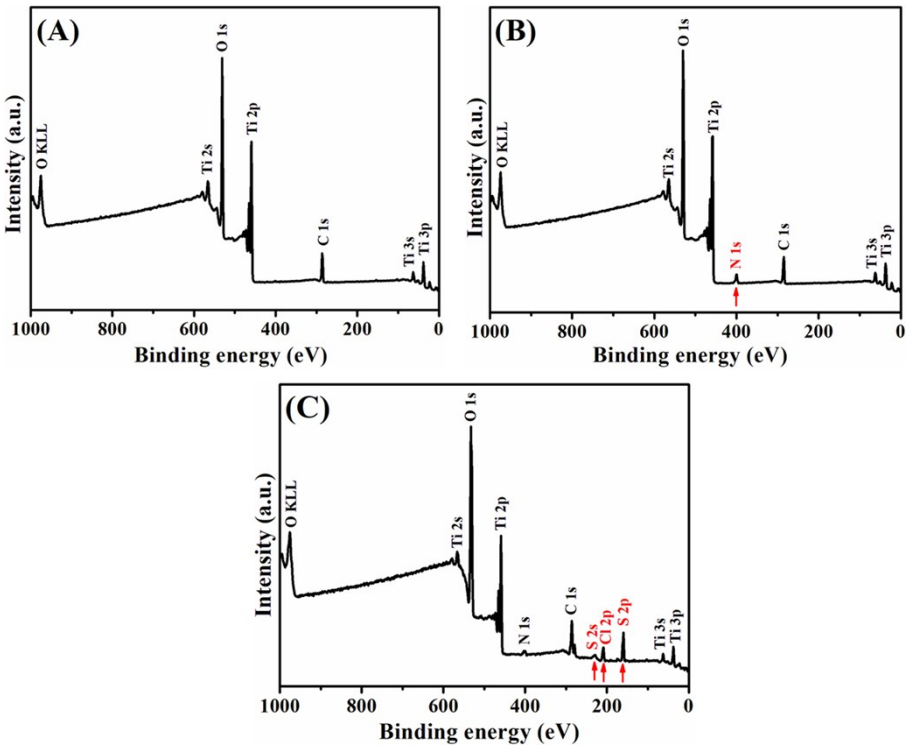

Fig. S1. Full-scan XPS spectra of the electrodes: (A) TiO_2-NTAs, (B) TiO_2-NTAs/g-C_3N_4, and (C) TiO_2-NTAs/g-C_3N_4/PEDOT.

Section 3: optimal conditions of the photoanode

The PEC property of the TiO_2-NTAs/g-C_3N_4/PEDOT photoanode was optimized by using a Pt-wire as working electrode and a modified TiO_2-NTAs electrode as counter electrode. Since the deposition rate of g-C_3N_4 and the thickness of PEDOT would affect photocurrent intensity of the photoanode, the dosage of urea for g-C_3N_4 deposition and the deposition cycle of PEDOT were mainly explored, as shown in Fig. S2.

Panel A of Fig. S2 shows photocurrent intensity of the TiO_2-NTAs/g-C_3N_4 electrode prepared with different dosages of urea during deposition process of g-C_3N_4. As the dosage of urea increased initially, the deposition of g-C_3N_4 on TiO_2-NTAs accumulated resulting in more light absorption and less surface defects,[2,7] and the photocurrent intensity enhanced. It could be seen that the dosage of 2.0 g urea reached the highest photocurrent intensity. After the dosage of urea further increased, the photocurrent intensity decreased slowly due to gradually increased surface recombination centers on the excessive of g-C_3N_4. Thus, 2.0 g urea was used for g-C_3N_4 deposition.

Panel B of Fig. S2 exhibits photocurrent intensity of the TiO_2-NTAs/g-C_3N_4/PEDOT electrode fabricated with different deposition cycles of PEDOT. As the deposition cycle of PEDOT increased to 3, the photocurrent intensity enhanced gradually due to increased amount of e□ective hole conductor of PEDOT coating on the electrode surface. After further increase in deposition cycle, the photocurrent intensity decreased, indicating that the PEDOT layer was too thick. The excessive PEDOT reduced the light absorption because of the increase of photon transmission distance.[8] Accordingly, 3 deposition cycle of PEDOT was applied to fabricated the photoanode.

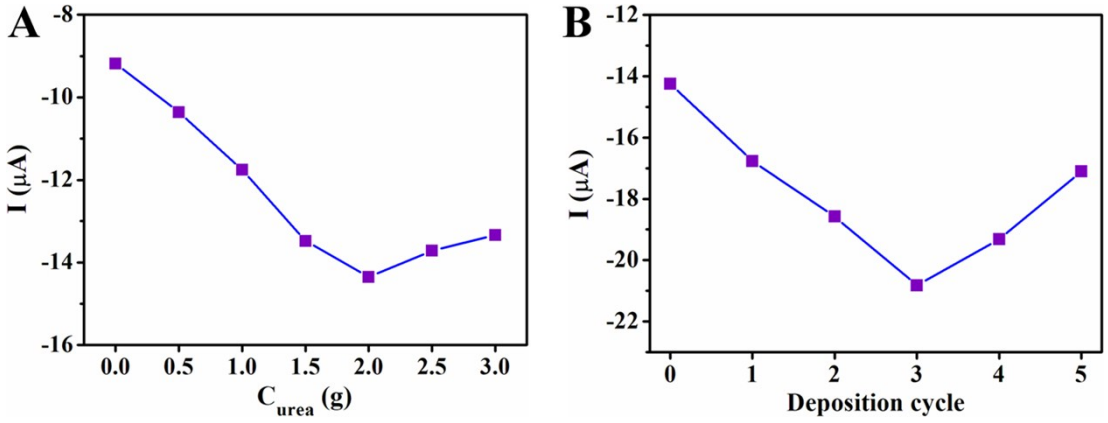

Fig. S2. Photocurrent responses of (A) the TiO_2-NTAs/g-C_3N_4 electrode prepared with different dosages of urea, and (B) TiO_2-NTAs/g-C_3N_4/PEDOT electrode fabricated with different deposition cycles of PEDOT.

Section 4: SEM of the cathodic sensor

The surface morphology of the cathodic sensing electrode for each fabrication step was shown in Fig. S3. It could be seen plenty of indium tin oxide nanoclusters was scattered on the bare ITO electrode (Panel A). After RGO electrodeposition, RGO nanosheets with plentiful wrinkles were covered on the electrode surface (Panel B). After CS modification, a gel-like film was observed on the electrode surface, and the outline of RGO nanosheets became blurred (Panel C). After Ab and BSA further immobilization, a large

number of larger-sized substances uniformly and tightly distributed on the electrode (Panel D). Thus, the morphology change in each SEM image illustrated successful assembly of the cathodic immunosensing electrode.

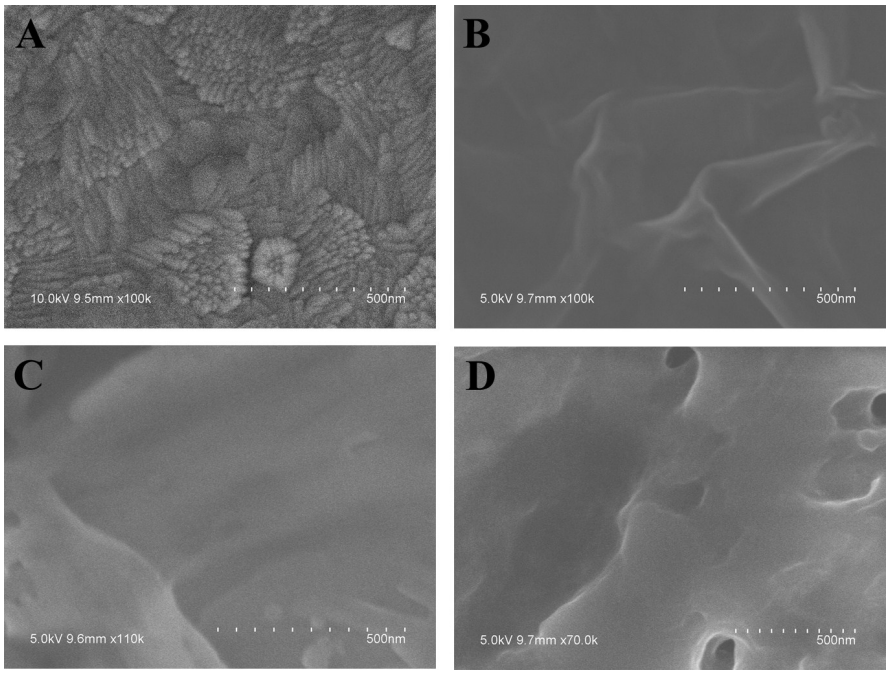

Fig. S3. SEM images of (A) the bare ITO electrode, (B) after RGO electrodeposition, (C) after CS modification, and (D) after Ab and BSA immobilization.

Section 5: EIS of the cathodic sensor

The fabrication process of the cathodic sensing electrode was characterized by EIS. As shown in Fig. S4, each impedance spectrum was composed of a semicircle at higher frequencies reflecting electron-transfer resistance and a linear part at low frequencies pointing the di□usion process. The semicircle diameter equals the electron-transfer resistance (R_{et}), which represents the restricted di□usion of the redox probe accessing the interface layer. For bare ITO electrode, the impedance spectrum presented a small R_{et} (curve a). After RGO electrodeposition, the R_{et} decreased owing to good electrical conductivity of RGO (curve b). After CS, Ab and BSA were subsequently immobilized onto the electrode in turn, gradually increased R_{et} was observed resulting from lower conductivity of CS layer as well as insulating effect of protein molecules (curve c-e). After the electrode was then incubated with target Ag, the R_{et} further increased (curve f), indicating the occurrence of the immunoreaction between target Ag and its Ab. Thus, the variation trend of the impedance spectra suggested successful fabrication of the cathodic immunosensing electrode.

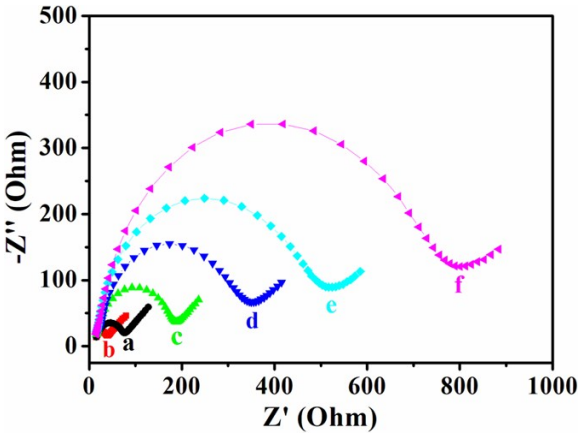

Fig. S4. EIS of (a) the bare ITO electrode, (b) after RGO electrodeposition, (c) after CS modification, (d) after Ab immobilization, (e) after BSA blocking, and (f) after incubation with 20 μL of 100 μg/mL Ag.

Section 6: general-utility, selectivity, repeatability, and stability

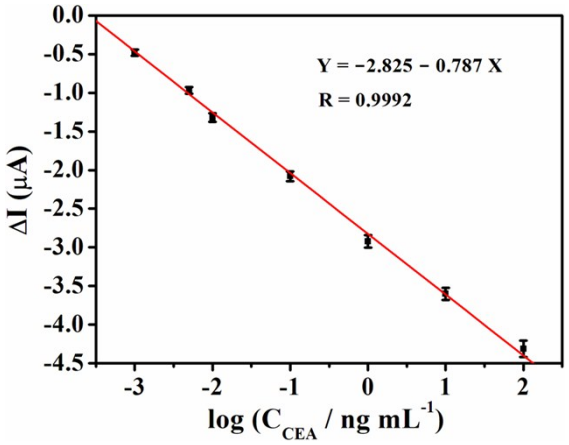

Fig. S5. Calibration curve of the PEC immunoassay for the detection of di□erent concentrations of CEA. $\Delta I = I_0 - I$; I_0 and I present photocurrent signals before and after specific immunoreaction, respectively.

To illustrate general-utility of the proposed self-powered PEC immunoassay separating photoanode from recognition event, the familiar biomarker of carcinoembryonic antigen (CEA) was selected as another target Ag and the capture probe was CEA antibody. The calibration curve of the PEC immunoassay toward CEA detection was shown in Fig. S5. The photocurrent signal weakened linearly with logarithm increase of the CEA concentration from 1 pg/mL to 100 ng/mL, and the limit of detection (S/N = 3) was calculated to be 0.3 pg/mL. As different biomarkers can specifically bind with different antibodies, the proposed self-powered PEC immunoassay is highly expected to detect other important biomarkers with both high sensitivity and anti-interference capability.

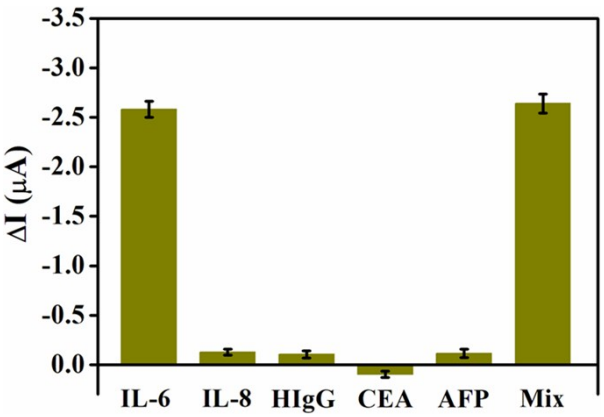

Fig. S6. Photocurrent signals of the PEC immunoassay for the detection of 10 ng/mL IL-6, IL-8, HIgG, CEA, AFP, and all their mixture, respectively. $\Delta I = I_0 - I$; I_0 and I are the photocurrent signals of the PEC immunoassay before and after specific immunoreaction. The error bars present the standard deviation of four parallel tests.

To verify whether the developed PEC immunoassay possesses well specificity, some familiar antigens including human interleukin-8 (IL-8), human IgG (HIgG), carcinoembryonic antigen (CEA), and α-fetoprotein (AFP) were inspected to challenge the PEC system. As shown in Fig. S6, comparing to the photocurrent signal tested with only IL-6, single interfering antigen or their mixture nearly has no evident change on photocurrent signal. Hence, the comparing results indicated that the photocurrent signal generated from the specific binding without obvious interference of nonspecific action.

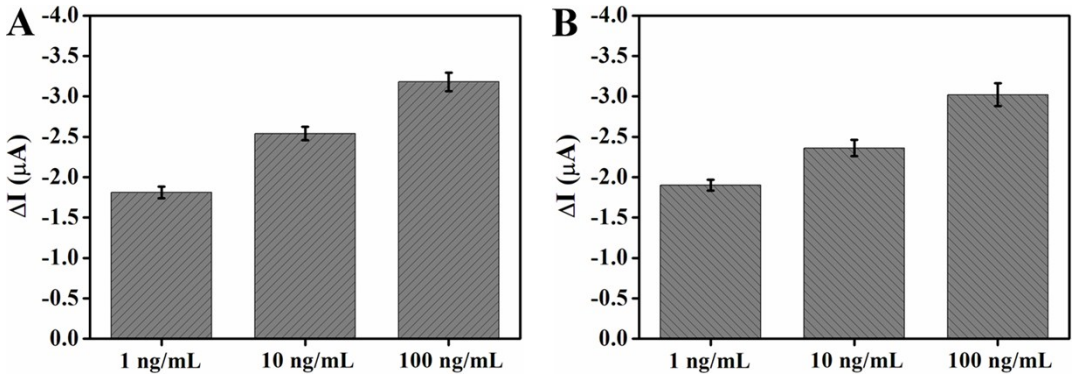

Fig. S7. (A) Intra-assay and (B) inter-assay on photocurrent signals of the cathodic PEC immunoassay for the detection of 1, 10, and 100 ng/mL of target Ag, respectively. $\Delta I = I_0 - I$; I_0 and I are the photocurrent signals of the PEC immunoassay before and after specific immunoreaction.

The repeatability of the cathodic PEC immunoassay was assessed with both intra-assay and inter-assay relative standard deviations (RSDs) of four parallel tests, as shown in Fig. S7. The calculating results exhibited that the intra-assay RSDs were 4.0%, 3.3%, and 3.6% for the detection of 1, 10, and 100 ng/mL

of target Ag, respectively; the inter-assay RSDs were 3.5%, 4.3%, and 4.7% by testing the same samples under the identical conditions. These results reflected a favorable precision and repeatability for the immunoassay.

The stability of the cathodic PEC immunoassay was evaluated by testing the photocurrent change of the sensing system. Two groups of sensing systems consisting of cathodic sensing electrode and photoanode were first prepared under the same conditions, and each group consisted of four sets of electrode systems. The photocurrent responses for the first group were tested without storage time, and the average photocurrent value was served as the initial value of the sensing system. After being stored at 4 °C in damp environment for a fortnight, the average photocurrent response of the second group of sensing systems maintained 95.3% of the initial value, showing good storage stability.

Section 7: References

1. Z. Zhang, P. Wang, *Energy Environ. Sci.* 2012, **5**, 6506−6512.
2. L. Liu, G. Zhang, J. T. S. Irvine, Y. Wu, *Energy Technol.* 2015, **3**, 982−988.
3. G. F. Samu, C. Visy, K. Rajeshwar, S. Sarker, V. R. Subramanian, C. Janáky, *Electrochim. Acta* 2015, **151**, 467−476.
4. W. S. Hummers Jr, R. E. Offeman, *J. Am. Chem. Soc.* 1958, **80**, 1339−1339.
5. T. T. Zheng, T. T. Tan, Q. F. Zhang, J. J. Fu, J. J. Wu, K. Zhang, J. J. Zhu, H. Wang, *Nanoscale* 2013, **5**, 10360−10368.
6. T. T. Li, X. Y. Li, Q. D. Zhao, Y. Shi, W. Teng, *Appl. Catal., B* 2014, **156−157**, 362−370.
7. M. Yang, J. Liu, X. Zhang, S. Qiao, H. Huang, Y. Liu, Z. Kang, *Phys. Chem. Chem. Phys.* 2015, **17**, 17887−17893.
8. B. Chong, W. Zhu, X. Hou, *J. Mater. Chem. A* 2017, **5**, 6233–6244.